Accuracy assessment of Beddoes-Leishman and IAG dynamic stall models for wind turbine applications

Journal of Physics: Conference Series **2767** (2024) 052053 doi:10.1088/1742-6596/2767/5/052053

Accuracy assessment of Beddoes-Leishman and IAG dynamic stall models for wind turbine applications

Omar Sherif Mohamed[1,a], **Pier Francesco Melani**[1,b], **Galih Bangga**[2,c], **Navid Aryan**[3,4,d], **Luca Greco**[4,e], **Alessandro Bianchini**[1,f]

[1] Department of Industrial Engineering, University of Florence, Via di Santa Marta 3, 50139, Florence, Italy.
[2] DNV, One Linear Park, Avon Street, Temple Quay, Bristol BS2 0PS, United Kingdom
[3] Department of Mechanical and Aerospace engineering (DIMA), Sapienza University of Rome, Via Eudossiana 18, 00184, Rome, Italy.
[4] CNR-INM - Institute of Marine Engineering, Via di Vallerano 139, 00128 Rome, Italy.

E-mail: [a]omar.sherif@unifi.it, [b]pierfrancesco.melani@unifi.it, [c]galih.bangga@dnv.com, [d]navid.aryan@uniroma1.it, [e]luca.greco@cnr.it, [f]alessandro.bianchini@unifi.it

Abstract. The study presents a systematic comparison between two of the most-credited dynamic stall models for wind turbine applications: the original Beddoes-Leishman (BL) model and the newly-developed IAG. The scope of such comparison, supported by experimental data, is to shed new light on the actual suitability of current dynamic stall models for their integration into modern wind turbine simulation codes, and on the best practices to calibrate them. Two different strategies are followed for the calibration of the BL model: 1) standard one, compliant with common practices found in the literature; 2) a physics-oriented one, focusing on the constants defining the dynamic stall onset as well as on the parameters governing the duration of the vortex shedding process. The IAG model, initially developed based on the first-order BL formulation and recently improved by reducing the number of constants and removing compressibility effects, is applied instead in its standard form only. The two models are compared across a range of oscillation mean angles, amplitudes, and reduced frequencies. Results demonstrate that the original BL model, although with a challenging calibration process, when properly tuned, can provide a very good description of aerodynamic unsteady loads. While showing consistent results, the IAG formulation appears to be more robust, as it employs fewer constants and extracts most of the needed information directly from the input polar data. The comparison between the calibrated BL and IAG models highlights critical modelling aspects, the computation of drag and determination of the stall onset above all, offering valuable insights for the future development of dynamic stall formulations.

1. Introduction

Dynamic stall is a phenomenon of primary interest in the design of modern wind turbines [1, 2]. Horizontal-axis rotors feature progressively longer and more flexible blades, rendering them susceptible to deformation-induced variations in the angle of attack [3]. This effect is strongly pronounced in the classical standstill instability under idling or parked conditions [4–7]. This susceptibility is compounded in floating offshore installations due to the platform's motion, influenced by wind, waves, and marine currents. Consequently, these environmental factors given the typically-used airfoils lead to the close-to-the-root blade sections surpassing the stall limit. The significance of dynamic stall models becomes more apparent in vertical-axis rotors, where angle of attack variations are intrinsic to the cycloidal motion of their blades, and surpassing the stall limit is inherent to the machine's behaviour [8, 9].

Among the dynamic stall models are those based on the Beddoes-Leishman (BL) formulation, a semi-empirical model originally developed for helicopter blades, and it follows an algorithm to compute accumulations of indicial responses based on arbitrary input [10, 11]. This model relies on the leading-edge pressure condition to predict stall onset, incorporates Kirchhoff theory to account for trailing-edge separation, and includes a process for vortex growth, convection, and flow reattachment. The original BL model has been refined and validated in the past for high Mach number [12] and wind turbine applications [13]. Several attempts have been made thereafter to modify the model for low Mach number conditions. For example, Hansen et al. [14] simplified the BL model for wind turbine applications by eliminating the compressibility and leading-edge separation effects. Sheng et al. [15] proposed a new stall onset criterion for low Mach number inflow, and in a subsequent work [16], they introduced a modification to model flow reattachment. Calabretta et al. [17] integrated the BL model into an aeroelastic tool for HAWTs, identifying pitch-down drag discrepancies. More recently, Boutet et al. [18] introduced further modifications for low Mach number applications, reporting some challenges related to the underestimation of lift overshoot and the overestimation of the pitching moment.

The IAG dynamic stall model has been developed specifically for wind turbine applications and tested against experimental data at various conditions [19, 20]. The first generation of the model is based on the first-order BL formulation [21]. Its robustness and applicability in the wind energy field have been further improved in the second generation by enabling a state-space formulation as well as removing the compressibility effects and decreasing the number of required constants. These developments, documented in [20], has brought improvements in the inviscid normal force coefficient (C_N) reconstruction as well as in the determination of chordwise and moment coefficients (C_C and C_M, respectively). The described model has been implemented in the wind turbine design package Bladed starting from version 4.14.0.2 and is used in the present computations.

In the present study, the limitations of the original BL formulation [21] are investigated by exploring the maximum achievable accuracy resulting from a proper calibration campaign tailored to wind turbine airfoils. The gain in accuracy is evaluated benchmarking the results with those provided by the standard BL (*i.e.*, following common practices from the literature), and the IAG model [20] against experimental data for the pitching S809 airfoil [22].

The paper is outlined as follows: Section 2 presents the mathematical formulation of both BL and IAG models, highlighting the main differences between them and the strategy used to calibrate the original BL model. In Section 3, the results for both models are presented and compared with the experimental measurements, demonstrating the effects of different implementations of the BL model and its calibration across some selected cases of different reduced frequencies, oscillation mean angles, and amplitudes. Finally, the conclusions of the study are drawn in Section 4.

2. Methodology

In this section, a brief description of the BL and IAG dynamic stall models is presented, emphasizing the differences between both models and the strategy employed for calibrating the BL model. This calibration enables a comparison among the standard BL with the constants suggested in the original model, the calibrated BL model, and the IAG model.

2.1. Description of the dynamic stall models

Both the BL and IAG rely on the same modelling strategy, where the coefficients of normal force (C_N), chord-wise (tangential) force (C_C), and pitching moment (C_M) are computed within three modules: *attached flow*, *separated flow*, and *vortex shedding*. The complete mathematical formulation for each model is not provided here as a detailed description of the BL model can be found in [10, 11], and for the IAG model (2nd generation), in [20]. In the following, the main differences between the proposed formulations are outlined (details are summarized in Table 1).

At the $n-th$ time step, the computation of C_{N_n} in the *attached flow* is carried out by both BL and IAG models by combining circulatory (superscript "C") and impulsive (superscript "I") load components and using as a forcing the change in time of the angle of attack, α_n (subscript "α"). For the evaluation of C^C_{N,α_n}, an effective angle of attack α_{E_n} is obtained from α_n by applying a certain amount of delay via the deficiency functions X^1_n and Y^1_n, which in turn depend on the empirical constants A_1, b_1, A_2, and b_2 (see Section 2.2). $C^I_{N,\alpha}$ is computed using the deficiency function D_{α_n}, dependent on the empirical constant K_α, which is also function of A_1, b_1, A_2, and b_2. The BL formulation considers an additional source of forcing, i.e., the non-dimensional pitch rate $q_n = \dot{\alpha}\frac{2V}{c}$, and has therefore two additional load components: $C^C_{N,q}$ and $C^I_{N,q}$, which are computed using the same approach of circulatory loads but different deficiency functions, (X^2_n, Y^2_n) and D_{q_n}, respectively. The same strategy is used for the pitching moment coefficient, which in the original BL model is computed as:

$$C_{M_n,BL} = [C^C_{M,\alpha_n} + C^I_{M,\alpha_n}] + [C^C_{M,q_n} + C^I_{M,q_n}] = [(0.25 - x_{AC}) \cdot C^C_{N,\alpha_n} - \tfrac{1}{M}(X^4_n + Y^4_n)] + [C^C_{M,q_n} + C^I_{M,q_n}] \quad (1)$$

The first part in square brackets of Eq. 1 refers to the load components due to α and depends on the position of the aerodynamic center x_{AC}, the freestream Mach number M, and the deficiency functions X^4_n and Y^4_n (for further details, please refer to [23]). In the IAG model, this is replaced by an added mass term as in Eq. 2, while the second part of Eq. 1 is ignored:

$$C_{M_n,IAG} = -\frac{\pi c \dot{\alpha}_n}{4V} \quad (2)$$

In the *separated flow* module, the BL model modifies the attached flow loads to account for the loss of circulation provoked by flow separation (the modified loads are identified by the superscript "f"). This is done based on the position of the unsteady separation point f_{2n}, according to Kirchhoff theory [24]. f_{2n} accounts for two effects. The first is a lag in the Leading Edge (LE) pressure peak with respect to the normal load under attached flow $C^P_N = C^C_{N_n} + C^I_{N_n}$, which is delayed via a deficiency function D_{P_n} as in Eq. 3:

$$C^{P1}_{N_n} = C^P_{N_n} - D_{P_n}(T_P) \quad (3)$$

Table 1: Comparison between the original BL and IAG model.

Feature	BL	IAG
General		
Compressibility effect	compressible	incompressible
Type of formulation	indicial	state-space
Drag correction	N/A	from static data and induced drag effects
Attached flow		
Forcing source	α and $q = \dot{\alpha}\frac{2V}{c}$	α
Impulsive normal force constants	$0.75K_\alpha$ and $0.75K_q$	K_α
C_M computation	semi-empirical correlation	from static data and added mass effects
Separated flow		
C_C & C_M computation	from static data at $\alpha(f_{2n})$	from static data at $\alpha(f_n)$
Vortex shedding		
Time constants T_v and T_f	vary based on LEV status	constant
Non-dimensional vortex time τ_v	$\tau_{v_{n-1}} + \frac{\Delta t}{c}V$	$\tau_{v_{n-1}} + 0.45\frac{\Delta t}{c}V$
Secondary vortex	computation of T_{st}	N/A

$C_{N_n}^{P1}$ is then used to compute the pressure-lagged angle of attack α_{f_n} and the corresponding separation point f_{1n}. The second is a lag due to the dynamic response of the boundary layer itself and is obtained by applying a further delay to f_{1n}:

$$f_{2n} = f_{1n} - D_{f_n}(T_f) \tag{4}$$

In Eqs. 3 and 4, T_P and T_f are two time constants subject to calibration (see Section 2.2). The IAG model adopts the same approach for the computation of $C_{N_n}^f$, but a different formulation for $C_{C_n}^f$ and $C_{M_n}^f$, which are calculated by directly plugging the pressure-lagged angle of attack α_{f_n} into static polar data, therefore ignoring the boundary layer dynamic term f_{2n}:

$$C_{C_n}^f = C_C^{VISC}(\alpha_{f_n}) \tag{5}$$

$$C_{M_n}^f = C_M^{VISC}(\alpha_{f_n}) \tag{6}$$

In both models the *vortex shedding* module is triggered during the pitch-up when the pressure-lagged normal force, $C_{N_n}^{P1}$ exceeds the critical normal force, C_N^{CRIT}, which is one of the key calibration parameters for the BL model (see Section 2.2). This results in the shedding of a so-called Leading Edge Vortex (LEV), which is responsible for additional load components, here referred to with the superscript "v". The normal force one $C_{C_n}^v$ is computed as:

$$C_N^v = \begin{cases} C_{N,n-1}^v \cdot \exp\left(-\frac{ds}{T_v}\right) + (C_{v,n} - C_{v,n-1}) \cdot \exp\left(-\frac{ds}{2T_v}\right), & \text{if } 0 \le \tau_v \le T_{v\ell} \text{ and pitch-up} \\ C_{N,n-1}^v \cdot \exp\left(-\frac{ds}{T_v}\right), & \text{otherwise} \end{cases} \tag{7}$$

where $C_{v,n} = C_{N_n}^C - C_{N_n}^f$ is the vortex lift, T_{vl} is the time required to the LEV to go over the airfoil chord, T_v is a time constant regulating vortex decay, and $ds = \frac{\Delta t}{c} V$ is the non-dimensional timestep. τ_{v_n} is a non-dimensional time tracking the instantaneous LEV position: in the BL model, it is computed as $\tau_{v_{n-1}} + ds$, in the IAG as $\tau_{v_{n-1}} + 0.45ds$. During vortex shedding, the time constants T_v and T_f are modified in the BL model according to the status of the LEV as per the strategy outlined in [21], while they remain constants in IAG. Moreover, in the BL formulation the chord-wise force coefficient $C_{C_n}^v$ is computed using a semi-empirical formula [13]:

$$C_{C_n}^v = k_{CC} + C_{C_n}^f \cdot f_{2n}^{D_{CC}(C_{N_n}^{P1} - C_N^{CRIT}) + (f_{2n} - f_n)} \tag{8}$$

where k_{CC} and D_{CC} are constants fitting the C_C curve in the post-stall region. Finally, the IAG model does not take the secondary vortex into account, whereas the BL model considers it via a characteristic shedding period (T_{st}), which is computed from the flow Strouhal number S_t (commonly taken equal to 0.19) via Eq. 9:

$$T_{st} = \frac{2(1 - f_{2n})}{St} \tag{9}$$

When $\tau_{v_n} > T_{vl} + T_{st}$, the vortex module is reset and a second vortex is shed.

Eventually, the lift coefficient C_{L_n} is derived in both models upon projection of the total C_{N_n} and C_{C_n}, coming from the sum of their respective components:

$$C_{L_n} = C_{N_n} \cos(\alpha_n) - C_{C_n} \sin(\alpha_n) \tag{10}$$

One of the key differences between them lies instead in the computation of the drag coefficient C_{D_n}. In the BL model, this is computed in the same manner as the lift, adding the zero-lift drag (C_{D_0}):

$$C_{D_n} = C_{D_0} + C_{N_n} \sin(\alpha_n) + C_{C_n} \cos(\alpha_n) \tag{11}$$

while the IAG model, a dedicated drag equation is adopted:

$$C_{D_n} = C_{D_n}^{VISC} + (\alpha_n - \alpha_{E_n})\, C_{N_n}^{C} + \left(C_{D_n}^{VISC} - C_{D_0}\right) \left[\left(\frac{1 - \sqrt{f_{2n}}}{2} \right)^2 - \left(\frac{1 - \sqrt{f^{VISC}}}{2} \right)^2 \right] + C_N^v \sin \alpha_n \tag{12}$$

where $C_{D_n}^{VISC}$ represents the static drag coefficient and f^{VISC} is the static separation position.

2.2. Calibration strategy for the BL model

Two different strategies are followed herein for the calibration of the model's constants. For simplicity, the default values (i.e., those coming from the application of the model in the literature) of the indicial constants (A_i, b_i) for the attached flow module, along with the static airfoil-dependent parameters extracted from static polar data, are used for all calibration sets.
In the *standard* one (namely, *BL Standard*), common practices from the literature are followed for the dynamic stall onset criterion, and the model time constants (T_P, T_f, T_v and T_{vl}). In practical terms, C_N^{CRIT} is computed from static data as the value of C_N corresponding to the point of maximum C_C. No tuning is applied to the fitting parameters of the static C_C curve, i.e., D_{CC} and k_{CC}, and to the model time constants, keeping the same values provided by Leishman and Beddoes for the NACA0012 airfoil [21]. The main assumption underlying this strategy is that these parameters do not change significantly with the airfoil shape.
In the *calibrated* one (*BL Calibrated*), a more physics-oriented approach is followed, focusing on:

- *constants defining the dynamic stall onset (C_N^{CRIT}, D_{CC}, k_{CC}):* these are calibrated to reproduce the static C_C curve in quasi-steady conditions, i.e., considering a low speed ramp variation of the angle of attack. C_N^{CRIT} is artificially raised until the model is able to match the position of the C_C peak, while D_{CC} and k_{CC} are tuned to best fit the static C_C curve in the post-stall region. As it will be shown in Section 3, this strategy is particularly effective for airfoils characterized by a more progressive stall mechanism dominated by flow separation from the Trailing Edge (TE) such as the S809;
- *parameters regulating the duration of the vortex shedding process (T_v, T_{vl}):* these are tuned based on the characteristics of the LEV shedding cycle, which in turn are inferred from the shape of the experimental nose-down C_M peak, as C_M is the most sensitive to variations in the LEV dynamic. T_{vl} is estimated from the timespan from the C_M break at stall to its negative maximum value, which corresponds to the LEV reaching the airfoil TE. T_v is increased, on the other hand, to closely match the C_M negative peak intensity.

An overview of the constants value coming from the the two strategies mentioned above are reported in Table 2.

Table 2: Values of the constants for the investigated dynamic stall models

Model	A_1	A_2	b_1	b_2	T_f	T_P	T_v	T_{vl}	C_N^{CRIT}	k_{CC}	D_{CC}
BL standard	0.3	0.7	0.14	0.53	3.0	1.7	6.0	11.0	0.84	0	8
BL calibrated	0.3	0.7	0.14	0.53	3.0	2.5	8.0	6.0	1.6	-0.06	1
IAG	0.3	0.7	0.7	0.53	3.0	1.7	6.0	6.0	0.84	N/A	N/A

3. Results and discussion

3.1. Test cases

The S809 airfoil pitching around its quarter-chord point at reduced frequency $k = \omega c/2V$ (being ω the pitching angular frequency, c the airfoil chord and V the incoming uniform flow velocity) is considered in the present work. For all the tested conditions, the Reynolds number is 1.0×10^6

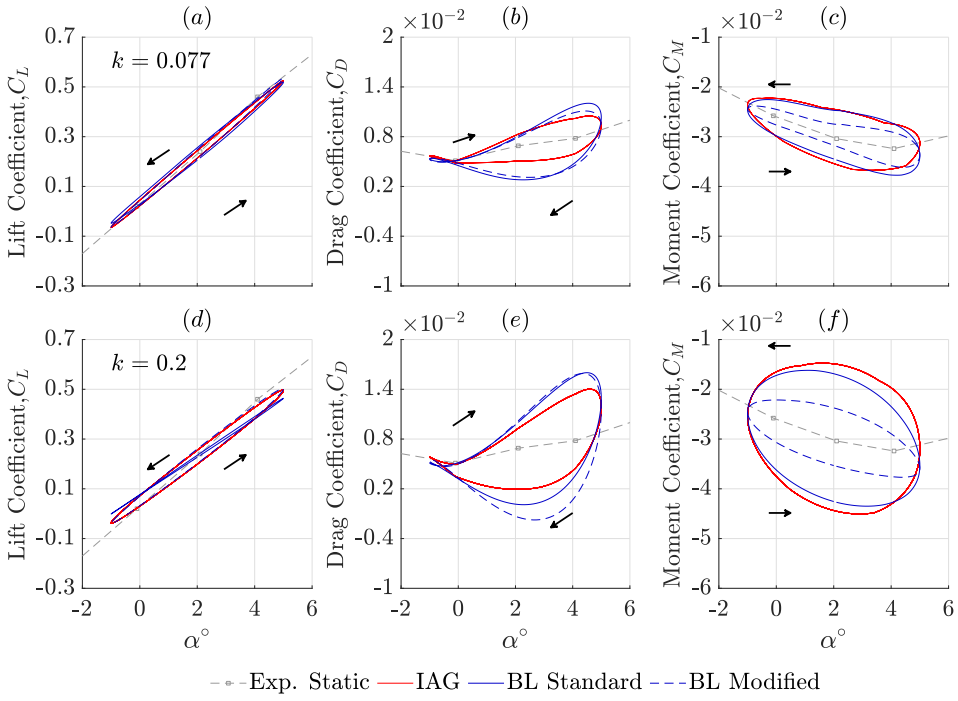

Figure 1: S809 airfoil sinusoidally pitching with amplitude $\alpha_A = 3^\circ$ and $\bar{\alpha} = 2^\circ$. Top: $k = 0.077$, bottom: $k = 0.2$.

and Mach number is 0.1. In the present analysis, the reduced frequency, the average angle of attack ($\bar{\alpha}$) and its amplitude (α_M) are varied to gain insight into the performance of the proposed models under specific flow conditions, thereby highlighting the differences between modelling strategies. A list of the proposed test cases is outlined in Table 3.

Table 3: Description of the test cases.

Case	$\bar{\alpha}$	α_M	k	Featured modules	Verification
A	2	3	0.077	Attached flow	Code-to-code
B	2	3	0.2	Attached flow	Code-to-code
C	8	10	0.077	Attached flow + separated flow	Code-to-code & experiment
D	14	10	0.077	Separated flow + vortex shedding	Code-to-code & experiment
E	20	10	0.077	Separated flow + vortex shedding	Code-to-code & experiment

3.2. Attached flow conditions

As outlined in Section 2.1, the BL and IAG models adopt different approaches in modelling the unsteady attached flow regime, particularly in two key aspects: the value of b_1 (0.7 for IAG and 0.14 for BL), and the inclusion of the non-dimensional pitching rate q. To understand the impact of these differences, an additional variation of the BL, referred to as *BL modified*[1], is introduced only in the *attached flow* results. In the latter, the effect of q is eliminated, and b_1 is adjusted to 0.7. Figure 1 shows the comparison between the different models for cases A and B and reduced frequencies $k = 0.077$ and $k = 0.2$. As there are no unsteady experimental results for these cases, only static data is reported as a reference. It must also be noted that, as the attached flow module is not involved in the calibration process (see Section 2.1), only the results for *BL standard* are reported here.

[1] Not to be confused with *BL calibrated*.

The lift hysteresis of *BL modified* and IAG match for both reduced frequencies, showing that the effect of compressibility, given the low Mach number considered, is negligible, while a major role is played by the constant b_1 and the inclusion of q. At low reduced frequency ($k = 0.077$), the impact of these two modifications is not relevant, as testified by the similarity between the BL (standard and modified) and the IAG curves. Differently, at $k = 0.2$, two trends in the behaviour of *BL standard* C_L curve can be observed: *i)* its slope is reduced, and the same occurs for the IAG model, although with a lower magnitude due to the higher b_1 value; *ii)* the amplitude of the lift hysteresis loop is notably reduced, especially when compared to the IAG one, which instead increases with the reduced frequency. This is attributed to the additional response due to the change in the pitching rate q, which, as pointed out by Leishman and Tyler [25], introduces a phase lead, partially compensating for the delay associated with the change in α. While this effect may be negligible in conventional wind turbine modeling, it becomes more relevant in some applications such as VAWTs, operating at notably higher reduced frequency.

Significant deviations between the models are observed, instead, for C_D and C_M, due to the use in the IAG of a different drag formulation (Eq. 12) and the added mass term (Eq. 2), respectively. The BL model exhibits a smooth C_D cycle with a significantly higher peak value compared to both the IAG model, which demonstrates, instead, constrained drag during pitching-up, followed by a sudden decrease before maintaining an almost constant value during the pitch-down phase. Regarding the added mass term, the fair agreement in terms of C_M between *BL standard* and IAG suggests that Eq. 2 also accounts for effect of q.

3.3. Separated and stalled flow validation

Investigations are further carried out for the S809 airfoil working under more challenging flow conditions. Three additional cases are herein considered focusing on the model characteristics under light- and deep-stall. The calculations are done by imposing the exact angle of attack measured during the experimental campaign [22], rather than the ideal, sinusoidal one, as suggested in [19].

The results for cases C, D, and E are reported in Fig. 2 to 4, respectively. Beside airfoil loads predictions, the plots show the absolute error of present predictions with respect to experimental data, in the pitch-up and pitch-down phases. As demonstrated by the error plots, in general the calibration process significantly enhances the BL model representation of experiments, particularly in shaping the C_D curve and determining the location and extension of the nose-down C_M peak in the deep-stall region. The effect of calibration on the predicted C_L behavior shows that the maximum lift value is significantly underestimated. The reason might lie in the formulation of the BL model, which has been developed for thin airfoils characterized by dominant LE separation and has inherent difficulty in handling TE separation (characterizing the stall behaviour of the S809). On the other hand, beside the reduced setup effort, the IAG model shows lower absolute errors and more accurately captures C_L overshoot. However, compared to the experiments, it underestimates lift production in the pre-stall phase and overestimates it in the re-attachment. It is notable that the IAG model is primarily designed to capture deep stall dynamics especially for design load case (DLC) 6.x family [6].

At $\bar{\alpha} = 8°$, under attached flow conditions consistent predictions are exhibited, with the two solvers matching the experimental results. At the onset of separation, however, the calibrated BL predicts an anticipated lift overshoot, in virtue of the C_N^{CRIT} value selected during the calibration process to define the stall onset. Differently, the IAG and standard BL models demonstrate a more accurate estimation of the experimental maximum lift. Notably, both *BL Calibrated* and IAG exhibit a more realistic drag hysteresis compared to *BL Standard*, which shows a significantly higher peak and a sharper drop during the pitch-down phase. Regarding pitching moment, the IAG and *BL Calibrated* outperform *BL Standard* during LEV formation. In the deep-stall region, however, they show higher nose-down C_M values compared to the *BL Standard* and better match the experimental measurements, as confirmed by the error plot.

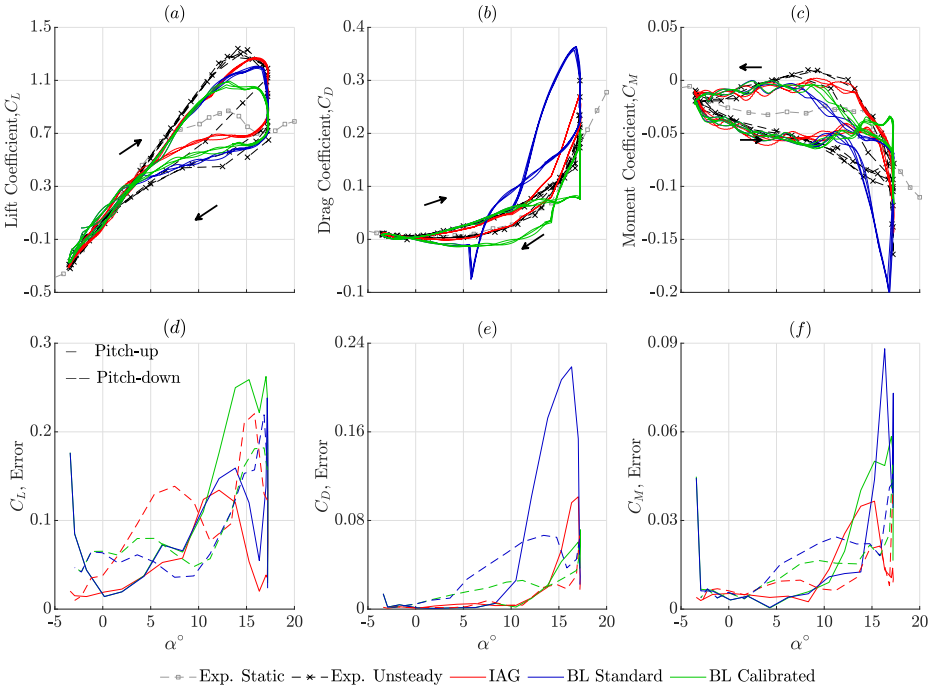

Figure 2: Unsteady characteristics of the S809 airfoil for $\alpha_A = 10°$ at $\bar{\alpha} = 8°$.

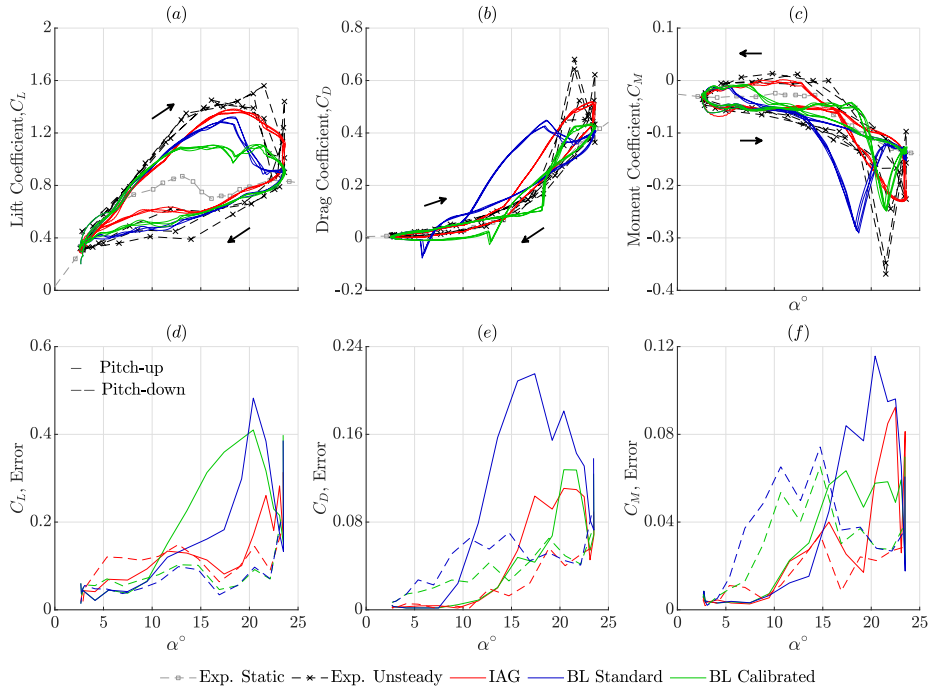

Figure 3: Unsteady characteristics of the S809 airfoil for $\alpha_A = 10°$ at $\bar{\alpha} = 14°$.

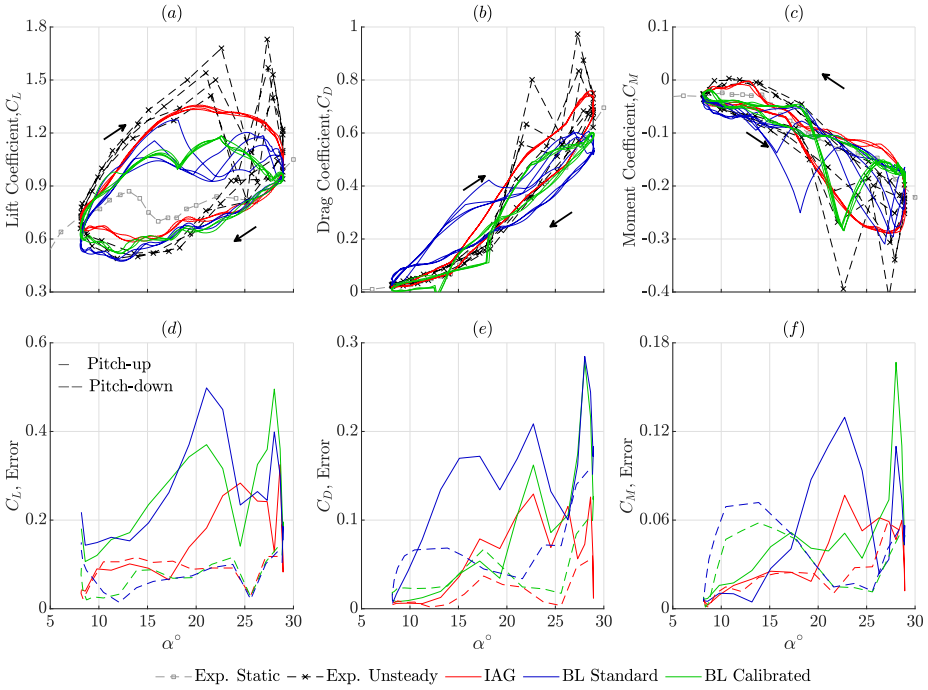

Figure 4: Unsteady characteristics of the S809 airfoil for $\alpha_A = 10^\circ$ at $\bar{\alpha} = 20^\circ$.

During flow reattachment, both *BL Calibrated* and IAG models demonstrate similar C_M results with smaller deviation from experiment with respect to *BL Standard*.

Moving to $\bar{\alpha} = 14^\circ$, the limited lift overshoot of the calibrated BL becomes more evident, showing a higher error during the pitch-up phase within the angle of attack range of $13^\circ < \alpha < 20^\circ$ compared to the standard BL. The latter exhibits a sudden drop in C_L at $\alpha \approx 18^\circ$. In general, both models show two lift peaks due to the secondary vortex shedding, which is not modelled in the IAG formulation. On the other hand, lift overshoot is well captured by IAG model. The drag coefficient loop illustrates the impact of the calibration process on BL model's performance, limiting the drag increase within $10^\circ < \alpha < 18^\circ$ compared to predictions by the standard BL. The IAG model shows a smoother C_D curve during pitch-up, with slightly higher C_D values compared to the experimental data. The pitching moment results indicate that the standard BL model experiences an early pitching moment break compared to the other models and experimental results, while the calibrated BL shows an overall lower error.

At $\bar{\alpha} = 20^\circ$, where the influence of vortex shedding on the airfoil behavior is maximum, the two lift peaks are more evident in the calibrated and standard BL models, while absent from the IAG one. However, the first lift overshoot is underestimated in the *BL standard* case, while the second occurs too early for *BL calibrated*. Similarly to cases C and D, the impact of the BL calibration is evident in the C_D hysteresis, damping the drag increase during the pitching up within $10^\circ < \alpha < 18^\circ$ for the calibrated BL compared with the standard one. On the other hand, the IAG shows a more accurate drag representation at higher angles of attack when compared to the experimental measurements. The pitching moment coefficient results show that the standard BL has an early pitching moment break point. The calibrated BL, on the other hand, yields an accurate reproduction of the C_M break point, similar to the IAG model.

4. Conclusions

The present study shows that, once properly set up, BL model can provide a good description of the unsteady loads for a complex airfoil such as the S809, although with clear limitations related to the class of airfoils it was originally conceived for. The comparison with the modern IAG model, requiring less calibration efforts and specifically designed for wind turbine airfoils,

highlights that:

- Under *attached flow* conditions, the difference between the BL and IAG formulations becomes relevant only at the higher reduced frequency, where the effects of the indicial response calibration, e.g., b_1, and of the pitch rate q cannot be neglected;
- In the light- and deep-stall regimes, the calibration of the BL model, in particular of the dynamic stall threshold C_N^{CRIT}, leads to a notable improvement in the reconstruction of the drag and pitching moment characteristics, at the cost of a loss of accuracy in terms of vortex lift magnitude.
- The dedicated drag formula in the IAG model allows it to compute a reliable drag hysteresis under different flow conditions. The vortex effects on drag during the pitch-up phase for the IAG model build slightly earlier than the experiment and this can be a subject for future improvement. On the other hand, the standard BL produced an overestimated drag during separation, however, if properly calibrated, it is capable of computing a more physically representative drag hysteresis.

From the comparison of the BL and IAG models, some critical modelling aspects are highlighted, thus providing useful information for the development of future dynamic stall formulations. Future studies will be aimed at assessing the performance of the models for higher reduced frequencies and different wind turbines airfoils and ultimately to verify their performance while included into full turbine simulation codes.

Acknowledgement
The participation of DNV was funded by the DNV research project grant "IEA Wind Task 47".

References

[1] Bangga G 2022 *Wind Turbine Aerodynamics Modeling Using CFD Approaches* (AIP Publishing LLC)
[2] Le Fouest S and Mulleners K 2022 *Renewable Energy* **198** 505–520
[3] Veers P, Bottasso C, Manuel L, Naughton J *et al.* 2023 *Wind Energy Science* **8** 1071–1131
[4] Wang K, Riziotis V A and Voutsinas S G 2017 *Wind Energy Science* **2** 415–437
[5] Garry Yuan Kwan G 2017 *TU Delft Master Thesis*
[6] Bangga G, Carrion M, Collier W and Parkinson S 2023 *Journal of Physics: Conference Series* **2626** 012026
[7] Chen C, Zhou J w, Li F and Zhai E 2022 *Renewable Energy* **187** 710–727
[8] Bianchini A, Bangga G, Baring-Gould I, Croce A *et al.* 2022 *Wind Energy Science* **7** 2003–2037
[9] Melani P F, Balduzzi F and Bianchini A 2021 *J. Eng. Gas Turbine. Power* **143** 111008
[10] Leishman J G and Beddoes T 1989 *Journal of the American Helicopter society* **34** 3–17
[11] Beddoes T 1982 *European Rotocraft Forum* **8**
[12] Johnson W *American Helicopter Society Annual Forum* **54**
[13] Gupta S and Leishman J G 2006 *Wind Energy* **9** 521–547
[14] Hansen M, Gaunaa M and Aagaard Madsen H 2004 *Risø-R-1354*
[15] Sheng W, Galbraith R M and Coton F 2006 *Journal of Solar Energy Engineering* **128**
[16] Sheng W, Galbraith R M and Coton F N 2007 *Journal of Aircraft* **44** 1856–1864
[17] Calabretta A, Molica Colella M, Greco L and Gennaretti M 2016 *Wind Energy* **19 (12)** 2301–2319
[18] Boutet J, Dimitriadis G and Amandolese X 2020 *Journal of Fluids and Structures* **93** 102852
[19] Bangga G, Lutz T and Arnold M 2020 *Wind Energy Science* **5** 1037–1058
[20] Bangga G, Parkinson S and Collier W 2023 *Energies* **16** 3994
[21] Leishman J and Beddoes T 1986 *42nd Forum of the American Helicopter Society*
[22] Ramsay R, Hoffman M and Gregorek G 1995 *NREL/TP-442-7817*
[23] Leishman J G 1988 *Journal of Aircraft* **25** 914–922
[24] Beddoes T 1983 *Vertica* **7**
[25] Tyler J C and Leishman J G 1992 *Journal of the American Helicopter Society* **37** 69–82